A&A 657, A96 (2022)
https://doi.org/10.1051/0004-6361/202142678

Astronomy & Astrophysics

Detection of the propargyl radical at λ 3 mm[⋆,⋆⋆]

M. Agúndez[1], N. Marcelino[2,3], C. Cabezas[1], R. Fuentetaja[1], B. Tercero[2,3], P. de Vicente[3], and J. Cernicharo[1]

[1] Instituto de Física Fundamental, CSIC, Calle Serrano 123, 28006 Madrid, Spain
e-mail: marcelino.agundez@csic.es; jose.cernicharo@csic.es
[2] Observatorio Astronómico Nacional, IGN, Calle Alfonso XII 3, 28014 Madrid, Spain
[3] Observatorio de Yebes, IGN, Cerro de la Palera s/n, 19141 Yebes, Guadalajara, Spain

Received 16 November 2021 / Accepted 9 December 2021

ABSTRACT

We report the detection of the propargyl radical (CH_2CCH) in the cold dark cloud TMC-1 in the λ 3 mm wavelength band. We recently discovered this species in space toward the same source at a wavelength of λ 8 mm. In those observations, various hyperfine components of the $2_{0,2}$–$1_{0,1}$ rotational transition, at 37.5 GHz, were detected using the Yebes 40 m telescope. Here, we used the IRAM 30 m telescope to detect ten hyperfine components of the $5_{0,5}$–$4_{0,4}$ rotational transition, lying at 93.6 GHz. The observed frequencies differ by 0.2 MHz with respect to the predictions from available laboratory data. This difference is significant for a radio-astronomical search for CH_2CCH in interstellar sources with narrow lines. We thus included the measured frequencies in a new spectroscopic analysis to provide accurate frequency predictions for the interstellar search for propargyl at millimeter wavelengths. Moreover, we recommend that future searches for CH_2CCH in cold interstellar clouds be carried out at λ 3 mm rather than at λ 8 mm. The $5_{0,5}$–$4_{0,4}$ transition is about five times more intense than the $2_{0,2}$–$1_{0,1}$ one in TMC-1, which implies that detecting the former requires about seven times less telescope time than detecting the latter. We constrain the rotational temperature of CH_2CCH in TMC-1 to 9.9 ± 1.5 K, which indicates that the rotational levels of this species are thermalized at the gas kinetic temperature. The revised value of the column density of CH_2CCH (including ortho and para species) is $(1.0 \pm 0.2) \times 10^{14}$ cm^{-2}, and thus the CH_2CCH/CH_3CCH abundance ratio is revised slightly higher, approaching one. This study opens the door to future detections of CH_2CCH in other cold interstellar clouds, making it possible to further investigate the role of this very abundant hydrocarbon radical in the synthesis of large organic molecules, such as aromatic rings.

Key words. astrochemistry – line: identification – molecular processes – ISM: molecules – radio lines: ISM

1. Introduction

The ongoing line surveys of the Taurus Molecular Cloud 1 (TMC-1) at the Green Bank Telescope (McGuire et al. 2020), GOTHAM, and at the Yebes 40 m telescope (Cernicharo et al. 2021d), QUIJOTE, are demonstrating that complex hydrocarbons, including cyclic and polycyclic aromatic ones, are formed in situ in cold dense clouds. Examples of such molecules detected toward TMC-1 are propylene (CH_2CHCH_3), vinyl and allenyl acetylene (CH_2CHCCH and $CH_2CCHCCH$), cyclopentadiene (c-C_5H_6), indene (c-C_9H_8), and benzyne (o-C_6H_4) (Marcelino et al. 2007; Cernicharo et al. 2021a,b,c,d; Burkhardt et al. 2021). Moreover, ethyl acetylene (CH_3CH_2CCH) and ethynyl benzene (c-C_6H_5CCH) have been tentatively detected (Cernicharo et al. 2021a,e), and there is strong evidence for the presence of aromatic rings such as benzene and naphthalene from the detection of their CN derivatives (McGuire et al. 2018, 2021; Cernicharo et al. 2021e).

It is not yet well understood which chemical routes are behind the formation of these aromatic cycles in cold dark clouds such as TMC-1. Hydrocarbon radicals are likely key players in the synthesis of these large molecules from smaller species. However, only a few such radicals have been detected. The methylidyne radical CH and the polyacetylenic radicals C_2H, C_3H, C_4H, and even longer ones have been known for a long time. Other radicals such as C_2H_3, C_3H_3, and C_3H_5 are likely important pieces in the synthesis of large hydrocarbons, but detecting them has proven to be difficult due to different possible reasons, such as spectral dilution due to the splitting of rotational lines into numerous fine and hyperfine components, a low abundance, a low dipole moment, or a lack of sufficiently sensitive radio-astronomical observations. We recently identified the propargyl radical (CH_2CCH) toward TMC-1 as part of the QUIJOTE line survey (Agúndez et al. 2021a). It was found that CH_2CCH is one of the most abundant radicals in TMC-1, being present at the level of its closed-shell counterpart CH_3CCH. Being that abundant, the propargyl radical could very well play an important role in the synthesis of aromatic molecules. For example, calculations indicate that the propargyl radical self-reaction can lead to cyclization, producing the aromatic radical phenyl radical at low temperatures (Miller & Klippenstein 2001; Zhao et al. 2021).

The radical CH_2CCH was detected in TMC-1 at λ 8 mm through six hyperfine components belonging to the $2_{0,2}$–$1_{0,1}$ rotational transition. Here we report the detection of CH_2CCH

⋆ Table A.1 is only available at the CDS via anonymous ftp to cdsarc.u-strasbg.fr (130.79.128.5) or via http://cdsarc.u-strasbg.fr/viz-bin/cat/J/A+A/657/A96

⋆⋆ Based on observations carried out with the Yebes 40 m telescope (projects 19A003, 20A014, 20D023, and 21A011) and the IRAM 30 m telescope. The 40 m radio telescope at Yebes Observatory is operated by the Spanish Geographic Institute (IGN; Ministerio de Transportes, Movilidad y Agenda Urbana). IRAM is supported by INSU/CNRS (France), MPG (Germany), and IGN (Spain).

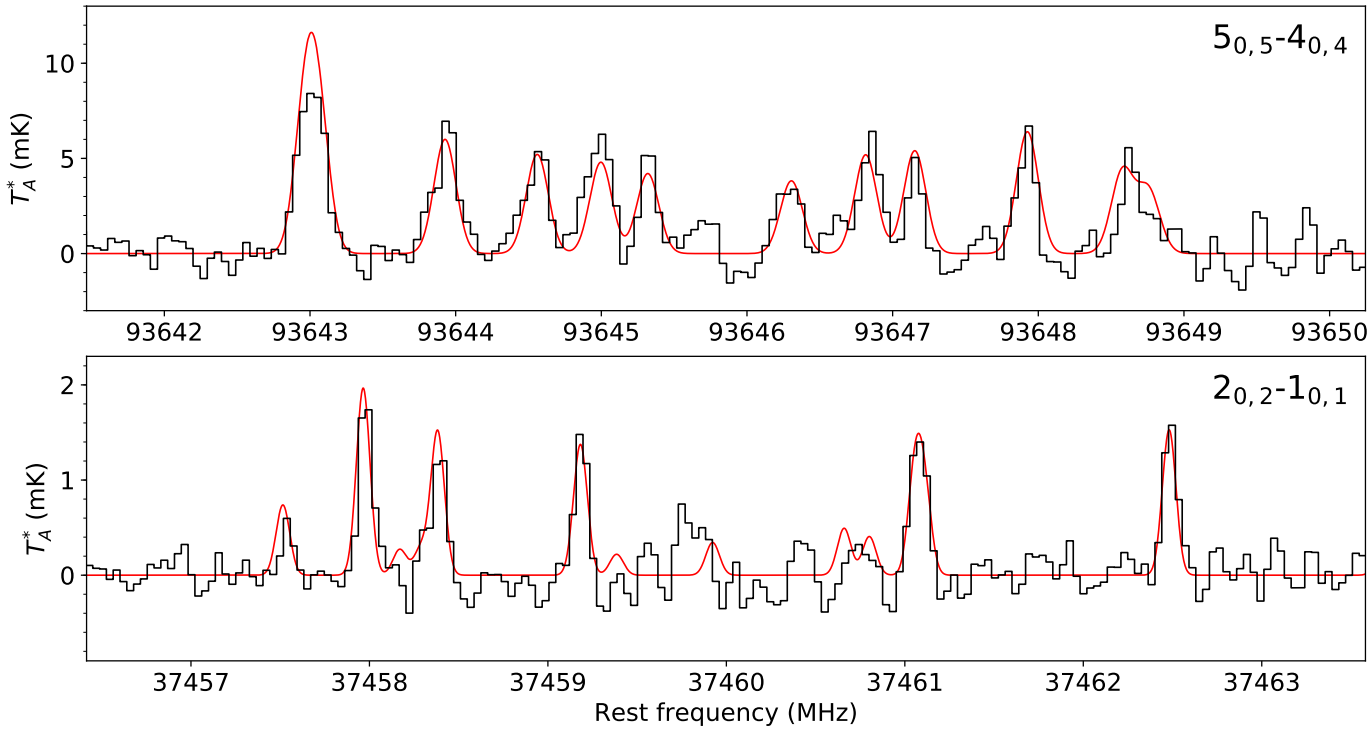

Fig. 1. Observed spectra of TMC-1 around the $2_{0,2}$–$1_{0,1}$ and $5_{0,5}$–$4_{0,4}$ rotational transitions of ortho CH_2CCH. The spectrum at 37.5 GHz is taken with the Yebes 40 m telescope (black histogram in the *bottom panel*), and that at 93.6 GHz is taken with the IRAM 30 m telescope (black histogram in the *top panel*). Transition quantum numbers, frequencies, and derived line parameters are given in Table 1. The synthetic spectra (red lines) were computed for a column density of ortho CH_2CCH of 7.5×10^{13} cm^{-2}, a rotational temperature of 9.9 K, an emission size of 40″ in radius, and a linewidth of 0.72 km s^{-1} for the $2_{0,2}$–$1_{0,1}$ lines and of 0.57 km s^{-1} for the $5_{0,5}$–$4_{0,4}$ lines (see text).

toward TMC-1 at λ 3 mm. We observed the $5_{0,5}$–$4_{0,4}$ transition in ten hyperfine components, with frequencies that differ by 0.2 MHz from previous available predictions. We thus used the observed frequencies to improve the spectroscopic parameters of CH_2CCH and provide accurate predictions to guide future astronomical searches. Moreover, the λ 3 mm line is about five times more intense than the λ 8 mm one, which suggests that the search for CH_2CCH in other cold dark clouds is more favorable in the λ 3 mm wavelength band.

2. Observations

The observations of TMC-1 at λ 3 mm were carried out using the IRAM (Institut de RadioAstronomie Millimétrique) 30 m telescope in September 2021. The observed position corresponds to the cyanopolyyne peak of TMC-1, $\alpha_{J2000} = 4^h41^m41.9^s$ and $\delta_{J2000} = +25°41'27.0''$. The 3 mm EMIR (Eight MIxer Receiver) receiver was used connected to a fast Fourier transform spectrometer, providing a spectral resolution of 48.84 kHz. We covered the spectral region around 93.6 GHz, where the $5_{0,5}$–$4_{0,4}$ rotational transition of CH_2CCH is located. We observed two setups at slightly different central frequencies in order to check for spurious signals, line emission from the image band, and other technical artifacts. The observations were performed in the frequency-switching observing mode with a frequency throw of 18 MHz, large enough to avoid possible contamination from negative frequency-switching artifacts arising from the different hyperfine components of CH_2CCH. Pointing scans were performed on strong and nearby quasars every 1–1.5 h, with pointing errors always within 3–5″. The antenna focus was checked every ∼6 h as well as at the beginning of each observing session and after sunrise. Weather conditions were between good and average for the northern hemisphere summer period, with opacities of 0.4–0.5 at 225 GHz and amounts of precipitable water vapor ranging from 1–3 mm to 6–7 mm. The spectra were calibrated in antenna temperature, T_A^*, corrected for atmospheric attenuation and for antenna ohmic and spillover losses, using the atmospheric transmission model ATM package (Cernicharo 1985; Pardo et al. 2001). The uncertainty in the calibration is estimated to be 10 %. System temperatures varied between 100 and 140 K, and the final T_A^* rms at 93.6 GHz is 1.1 mK after 31.4 h of total on-source telescope time.

The final spectrum shown in Fig. 1 was obtained after averaging the data taken in September 2021 with previous spectra from our TMC-1 3 mm line survey (Marcelino et al. 2007; Cernicharo et al. 2012). At the frequency of the $5_{0,5}$–$4_{0,4}$ transition of CH_2CCH, the observed time in the survey data is 4.0 h. Including these data has improved the final sensitivity down to 0.9 mK, resulting in a total on-source integration time of 35.4 h for each polarization (twice this value after averaging the two polarizations).

We also present a more sensitive spectrum of TMC-1 at the frequency of the $2_{0,2}$–$1_{0,1}$ transition of CH_2CCH, 37.5 GHz, with respect to that presented by Agúndez et al. (2021a). New data were gathered in several observing sessions between January and May 2021. These data are part of the ongoing QUIJOTE line survey that is being carried out with the Yebes 40 m telescope. The line survey uses a 7 mm receiver that covers the *Q* band, from 31.0 to 50.3 GHz, with horizontal and vertical polarizations. A detailed description of the system is given by Tercero et al. (2021). Receiver temperatures in the observing sessions carried out in 2020 vary from 22 K at 32 GHz to 42 K at 50 GHz. Some power adaptation in the down-conversion chains carried out in 2021 reduced the receiver temperatures to 16 K at

Table 1. Observed line parameters of CH_2CCH in TMC-1.

Transition [a]				ν_{calc} [b] (MHz)	ν_{obs} [c] (MHz)	Δv [d] (km s^{-1})	T_A^* peak (mK)	$\int T_A^* dv$ (mK km s^{-1})	S/N [e] (σ)
$2_{0,2}$–$1_{0,1}$	J = 3/2–1/2	F_1 = 2–1	F = 2–1	37457.515	37457.542(20)	0.55(35)	0.60	0.35(22)	4.5
$2_{0,2}$–$1_{0,1}$	J = 5/2–3/2	F_1 = 3–2	F = 4–3	37457.965	37457.981(10)	0.71(16)	1.92	1.45(27)	16.4
$2_{0,2}$–$1_{0,1}$	J = 5/2–3/2	F_1 = 2–1	F = 3–2	37458.382	37458.390(13)	0.80(27)	1.28	1.09(29)	11.6
$2_{0,2}$–$1_{0,1}$	J = 5/2–3/2	F_1 = 3–2	F = 3–2	37459.186	37459.187(10)	0.65(14)	1.58	1.09(22) [f]	12.9
$2_{0,2}$–$1_{0,1}$	J = 5/2–3/2	F_1 = 2–1	F = 2–1	37461.057	37461.078(11)	0.85(15)	1.53	1.38(25) [g]	14.3
$2_{0,2}$–$1_{0,1}$	J = 5/2-3/2	F_1 = 2-1	F = 2–1	37461.111					
$2_{0,2}$–$1_{0,1}$	J = 3/2–1/2	F_1 = 2–1	F = 3–2	37462.481	37462.489(10)	0.76(17)	1.63	1.31(25)	14.3
$5_{0,5}$–$4_{0,4}$	J = 11/2–9/2	F_1 = 6–5	F = 7–6	93642.970	93643.011(15)	0.69(11)	9.00	6.60(93) [g]	22.3
$5_{0,5}$–$4_{0,4}$	J = 11/2–9/2	F_1 = 5–4	F = 6–5	93643.059					
$5_{0,5}$–$4_{0,4}$	J = 11/2–9/2	F_1 = 6–5	F = 6–5	93643.927	93643.940(22)	0.65(18)	6.25	4.32(97)	15.1
$5_{0,5}$–$4_{0,4}$	J = 11/2–9/2	F_1 = 6–5	F = 5–4	93644.560	93644.557(28)	0.66(24)	4.98	3.51(99)	12.1
$5_{0,5}$–$4_{0,4}$	J = 11/2–9/2	F_1 = 5–4	F = 5–4	93644.997	93644.982(22)	0.65(16)	6.19	4.30(92)	15.0
$5_{0,5}$–$4_{0,4}$	J = 11/2–9/2	F_1 = 5–4	F = 4–3	93645.319	93645.325(18)	0.38(14)	5.76	2.34(71)	10.7
$5_{0,5}$–$4_{0,4}$	J = 9/2–7/2	F_1 = 4–3	F = 4–3	93646.305	93646.286(48)	0.61(30)	3.68	2.40(114)	8.6
$5_{0,5}$–$4_{0,4}$	J = 9/2–7/2	F_1 = 4–3	F = 5–4	93646.815	93646.849(31)	0.61(32)	5.73	3.72(136)	13.4
$5_{0,5}$–$4_{0,4}$	J = 9/2–7/2	F_1 = 5–4	F = 5–4	93647.152	93647.155(25)	0.35(17)	5.13	1.89(87)	9.0
$5_{0,5}$–$4_{0,4}$	J = 9/2–7/2	F_1 = 5–4	F = 6–5	93647.925	93647.919(24)	0.44(18)	6.36	2.99(103)	12.7
$5_{0,5}$–$4_{0,4}$	J = 9/2–7/2	F_1 = 5–4	F = 4–3	93648.580	93648.648(41)	0.62(45)	4.65	3.07(145) [g]	11.0
$5_{0,5}$–$4_{0,4}$	J = 9/2–7/2	F_1 = 4–3	F = 3–2	93648.750					

Notes. The line parameters ν_{obs}, Δv, T_A^* peak, and $\int T_A^* dv$ as well as the associated errors were derived from a Gaussian fit to each line profile. [a] Quantum numbers from the coupling scheme of Tanaka et al. (1997). [b] Calculated frequencies, ν_{calc}, from the combined laboratory and astronomical fit carried out in this work. [c] Observed frequencies adopting a systemic velocity of 5.83 km s^{-1} for TMC-1 (Cernicharo et al. 2020). [d] Δv is the full width at half maximum. [e] The signal-to-noise ratio is computed as $S/N = \int T_A^* dv$ / [rms $\times$ $\sqrt{\Delta v \times \delta v (c/\nu_{calc})}$], where c is the speed of light and δv is the spectral resolution. For the lines observed with the Yebes 40 m telescope at 37.5 GHz, δv = 0.03815 MHz and rms = 0.19 mK, while for the lines observed with the IRAM 30 m telescope at 93.6 GHz, δv = 0.04884 MHz and rms = 0.9 mK. The rest of the parameters are given in the table. [f] Line overlaps with the $2_{1,2}$–$1_{1,1}$ transition of *syn*-C_2H_3OH, which lies at 37459.184 MHz (see Agúndez et al. 2021b). The observed intensity is thus the sum of the CH_2CCH and the *syn*-C_2H_3OH lines. [g] Observed line results from a blend of two unresolved hyperfine components.

32 GHz and 25 K at 50 GHz. The backends are 2 × 8 × 2.5 GHz fast Fourier transform spectrometers with a spectral resolution of 38.15 kHz, providing the whole coverage of the Q band in both polarizations. The QUIJOTE observations were performed using the frequency-switching observing mode with a frequency throw of 10 MHz in the very first observing runs, which took place in November 2019 and February 2020, and 8 MHz in the later ones. The main beam efficiency of the Yebes 40 m telescope varies from 0.6 at 32 GHz to 0.43 at 50 GHz. The intensity scale used in this work, antenna temperature (T_A^*), was calibrated using two absorbers at different temperatures and the ATM package (Cernicharo 1985; Pardo et al. 2001). Calibration uncertainties were adopted to be 10%. After including all data taken between November 2019 and May 2021, the total on-source telescope time is 238 h in each polarization (twice this value after averaging the two polarizations). The IRAM 30 m and Yebes 40 m data were analyzed using the GILDAS software[1].

3. Results and discussion

3.1. Improved rotational spectroscopy for CH_2CCH

The rotational spectrum of the propargyl radical has been measured in the laboratory at frequencies below 38 GHz by Tanaka et al. (1997). Due to the existence of two equivalent H nuclei, the radical has ortho and para statistics. Ortho levels have K_a even, and para levels have K_a odd. The statistical ortho-to-para ratio is three. The dipole moment of CH_2CCH has been calculated by Botschwina et al. (1995) to be 0.14 D, while more recently Küpper et al. (2002) measured a value of 0.150 ± 0.005 D, which is the value we adopt hereafter.

Our IRAM 30 m data of TMC-1 show a group of lines spanning 6 MHz around 93646 MHz (see the top panel in Fig. 1), which we assign to the hyperfine components of the $5_{0,5}$–$4_{0,4}$ transition of CH_2CCH. The measured frequencies are systematically shifted up by 0.2 MHz with respect to the predicted frequencies in the Cologne Database for Molecular Spectroscopy (CDMS; Müller et al. 2005)[2]. The entry in the CDMS is based on a fit to the laboratory frequencies measured by Tanaka et al. (1997). These authors measured the fine and hyperfine structure of the rotational transitions $1_{0,1}$–$0_{0,0}$, $2_{0,2}$–$1_{0,1}$, $2_{1,2}$–$1_{1,1}$, and $2_{1,1}$–$1_{1,0}$, lying at 18.7 GHz and in the 37–38 GHz range. Although the experimental accuracy is quite good, a few kilohertz, the limited range of J values covered means that when extrapolating to the λ 3 mm wavelength band, the frequency errors could be significant for radio-astronomical purposes. The CDMS quotes frequency errors of just ~55 kHz for the hyperfine components of the $5_{0,5}$–$4_{0,4}$ transition, although our TMC-1 observations show that the error is in fact as high as ~200 kHz.

[1] http://www.iram.fr/IRAMFR/GILDAS/

[2] https://cdms.astro.uni-koeln.de/

This is significant for a radio-astronomical search for CH_2CCH in sources with narrow lines, such as TMC-1.

In order to obtain more accurate frequency predictions for CH_2CCH, we carried out a new spectroscopic analysis using the SPFIT program (Pickett 1991) and including the laboratory frequencies of Tanaka et al. (1997) and the astronomical frequencies measured in TMC-1 for the ten hyperfine components of the $5_{0,5}$–$4_{0,4}$ transition (see the derived line parameters in Table 1). The Hamiltonian used for the analysis is the same as that employed by Tanaka et al. (1997) and has the following form:

$$H = H^{\rm rot} + H^{\rm cd} + H^{\rm sr} + H^{\rm mhf}, \quad (1)$$

where $H^{\rm rot}$ and $H^{\rm cd}$ contain the rotational and centrifugal distortion parameters, respectively, $H^{\rm sr}$ is the spin-rotation term, and $H^{\rm mhf}$ represents the magnetic hyperfine coupling interaction between the unpaired electron and the hydrogen nuclei. A complete description of these terms can be found in Tanaka et al. (1997). The coupling scheme used is $\mathbf{J} = \mathbf{N} + \mathbf{S}$, $\mathbf{F}_1 = \mathbf{J} + \mathbf{I}_1$, and $\mathbf{F} = \mathbf{F}_1 + \mathbf{I}_2$, where $\mathbf{I}_1 = \mathbf{I}(\mathrm{H_a})$ and $\mathbf{I}_2 = \mathbf{I}(\mathrm{H_{m1}}) + \mathbf{I}(\mathrm{H_{m2}})$. The radical CH_2CCH has two equivalent H nuclei, the methylenic ones, and the hyperfine interaction term H^{mhf} is thus written explicitly as a two spin system:

$$H^{mhf} = a_F^{(\mathrm{H_a})} \cdot \mathbf{S} \cdot \mathbf{I}_1 + \mathbf{I}_1 \cdot \mathbf{T}^{(\mathrm{H_a})} \cdot \mathbf{S} + a_F^{(\mathrm{H_{m1}},\mathrm{H_{m2}})} \cdot \mathbf{S} \cdot \mathbf{I}_2 + \mathbf{I}_2 \cdot \mathbf{T}^{(\mathrm{H_{m1}},\mathrm{H_{m2}})} \cdot \mathbf{S}, \quad (2)$$

where $a_F^{(\mathrm{H_a})}$ and $\mathbf{T}^{(\mathrm{H_a})}$ stand for the Fermi contact constant and the dipole-dipole interaction tensor for the acetylenic hydrogen nucleus, respectively, and $a_F^{(\mathrm{H_{m1}},\mathrm{H_{m2}})}$ and $\mathbf{T}^{(\mathrm{H_{m1}},\mathrm{H_{m2}})}$ are averages of the coupling constants for the two methylenic hydrogen nuclei that are equivalent. In this manner, each energy level is denoted by six quantum numbers: N, K_a, K_c, J, F_1, and F.

The results obtained from the fit are shown in Table 2, where they are compared with those reported by Tanaka et al. (1997). As expected, the new derived parameters for CH_2CCH are almost identical to those reported before. The inclusion of the $5_{0,5}$–$4_{0,4}$ transition in the fit only affects the rotational constants B and C and the distortion constants Δ_N and Δ_{NK}. For B, C, and Δ_{NK} the differences are smaller than the 3σ uncertainties. However, for the Δ_N distortion constant the difference is much larger, as expected, due to the inclusion of rotational transitions with higher quantum number N. We used the spectroscopic parameters obtained in this work for CH_2CCH to obtain accurate frequency predictions at millimeter wavelengths. The catalog file with the predicted frequencies and the calculated intensities at 300 K is provided in Table A.1 at the CDS. The intensities are calculated adopting a dipole moment of 0.150 D, the experimental value measured by Küpper et al. (2002). The rotational partition functions used in these predictions are listed at different temperatures in Table 3. The rotational partition function was calculated considering a maximum value of 30 for the quantum number N.

3.2. Excitation and abundance of CH_2CCH in TMC-1 and guidance for further searches

We also present the observed spectrum of TMC-1 at the frequency of the $2_{0,2}$–$1_{0,1}$ transition of CH_2CCH (see the bottom panel in Fig. 1). This spectrum is more sensitive than that presented in Agúndez et al. (2021a) because it includes additional observations taken with the Yebes 40 m telescope. The rms noise level between their and our observations decreased from 0.30 to 0.19 mK per 38.15 kHz channel. As a consequence, the CH_2CCH lines are now more clearly detected. The new line parameters derived for the six hyperfine components of the $2_{0,2}$–$1_{0,1}$ transition of CH_2CCH are given in Table 1.

As can be seen in Fig. 1, the strongest hyperfine component of the $5_{0,5}$–$4_{0,4}$ transition is about five times more intense than the strongest component of the $2_{0,2}$–$1_{0,1}$. This is consistent with the rotational temperature of CH_2CCH being close to the gas kinetic temperature of TMC-1, ~10 K (Fehér et al. 2016). At this temperature, the $5_{0,5}$ rotational level, with an energy of ~13.5 K, is expected to be more populated than the $2_{0,2}$ level, which has an energy of ~2.7 K. In addition, the Einstein coefficient of spontaneous emission is about 20 times larger for the $5_{0,5}$–$4_{0,4}$ transition than for the $2_{0,2}$–$1_{0,1}$. These facts make the $5_{0,5}$–$4_{0,4}$ transition at 93.6 GHz more favorable for detection than the $2_{0,2}$–$1_{0,1}$ transition at 37.5 GHz. Indeed, if we assume typical values for the system temperatures, $T_{\rm sys}$ = 40 K at 37.5 GHz with the Yebes 40 m telescope and $T_{\rm sys}$ = 120 K at 93.6 GHz with the IRAM 30 m telescope, and we keep in mind that the

Table 2. Spectroscopic parameters of CH_2CCH (in MHz).

Parameter	Global Fit	Tanaka et al. (1997)
A	288 055 [(a)]	288 055
B	9523.6746(41)	9523.6775(60)
C	9206.8776(41)	9206.8805(60)
Δ_N	0.003004(72)	0.003440(63)
Δ_{NK}	0.3758(28)	0.3753(28)
Δ_K	22.62 [(a)]	22.62
δ_N	0.000103 [(a)]	0.000103
δ_K	0.1575 [(a)]	0.1575
ε_{aa}	−529.386(60)	−529.386(60)
ε_{bb}	−11.524(31)	−11.524(30)
ε_{cc}	−0.520(31)	−0.520(30)
$a_F^{(\mathrm{H_a})}$	−36.322(25)	−36.323(24)
$T_{aa}^{(\mathrm{H_a})}$	17.400(26)	17.400(24)
$T_{bb}^{(\mathrm{H_a})}$	−17.220(38)	−17.220(37)
$a_F^{(\mathrm{H_m})}$	−54.20(12)	−54.21(11)
$T_{aa}^{(\mathrm{H_m})}$	−14.122(20)	−14.121(19)
$T_{bb}^{(\mathrm{H_m})}$	12.88 [(a)]	12.88
rms [(b)]	6.3	7.0
N [(c)]	55	46

Notes. Numbers in parentheses are 3σ uncertainties in units of the last digits. $\mathrm{H_a}$ and $\mathrm{H_m}$ refer to the acetylenic and methylenic hydrogen nuclei, respectively. [(a)] Parameter fixed to the value reported by Tanaka et al. (1997). [(b)] Standard deviation of the fit (in kHz). [(c)] Number of lines included in the fit.

Table 3. Rotational partition function (Q_r) of CH_2CCH at different temperatures.

Temperature (K)	Q_r
9.375	294.5
18.750	718.9
37.500	1959.3
75.000	5506.5
150.000	14 710.5
225.000	24 377.0
300.000	33 479.9

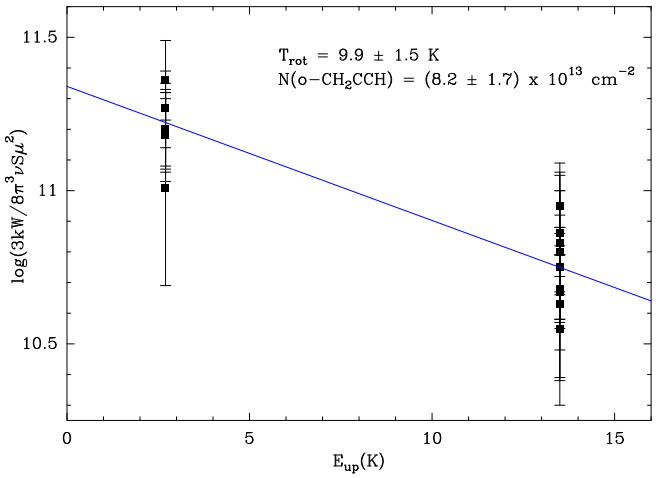

Fig. 2. Rotation diagram of ortho CH_2CCH in TMC-1.

line at 93.6 GHz is five times more intense than the 37.5 GHz line, the radiometer equation tells us that in order to detect the two lines with the same signal-to-noise ratio (S/N), one must invest ∼7 times more integration time at the Yebes 40 m telescope than with IRAM 30 m telescope. The fact that in our data the $2_{0,2}$–$1_{0,1}$ transition is detected with a similar or even higher S/N than the $5_{0,5}$–$4_{0,4}$ transition (see Table 1) is a consequence of the much longer integration time invested with the Yebes 40 m telescope (238 h) compared to that employed for the IRAM 30 m spectrum (35.4 h). In summary, the rotational transitions in the λ 3 mm wavelength band, in particular the $5_{0,5}$–$4_{0,4}$ at 93.6 GHz (see below), are the most favorable for detection and should be the target in future searches for CH_2CCH in cold dark clouds.

The availability of two rotational transitions with different upper level energies allows us to constrain the rotational temperature of the propargyl radical in TMC-1. We built a rotation diagram using the velocity-integrated intensities given in Table 1, and we derive a rotational temperature of 9.9 ± 1.5 K (see Fig. 2). We therefore confirm the assumption made by Agúndez et al. (2021a) that the rotational levels of CH_2CCH are thermalized at the gas kinetic temperature of TMC-1, ∼10 K (Fehér et al. 2016). This fact is expected based on the low dipole moment of CH_2CCH (0.150 D; Küpper et al. 2002), which implies low critical densities, probably a few 10^2 cm^{-3} (i.e., well below the volume density of H_2 in TMC-1, a few 10^4 cm^{-3}; Pratap et al. 1997; Cordiner et al. 2013). The column density derived from the rotation diagram for ortho CH_2CCH is $(8.2 \pm 1.7) \times 10^{13}$ cm^{-2}. A more precise determination of the column density can be obtained by fitting the observed spectra with synthetic spectra calculated under local thermodynamic equilibrium. For this calculation we adopted a rotational temperature of 9.9 K, as derived from the rotation diagram, a full width at half maximum of 0.72 km s^{-1} for the $2_{0,2}$–$1_{0,1}$ lines and 0.57 km s^{-1} for the $5_{0,5}$–$4_{0,4}$ lines, which are the arithmetic mean of the values derived for the hyperfine components of each transition (see Table 1), and assumed that the emission is distributed in the sky as a circle with a radius of 40″, as observed for various hydrocarbons in TMC-1 (Fossé et al. 2001). The observed spectra at 37.5 GHz and 93.6 GHz are well reproduced when adopting a column density of 7.5×10^{13} cm^{-2} (see Fig. 1). Assuming an ortho-to-para ratio of three, the column density of CH_2CCH (including ortho and para) in TMC-1 is $(1.0 \pm 0.2) \times 10^{14}$ cm^{-2}, which is slightly higher than the value derived previously by Agúndez et al. (2021a). The column density of the closed-shell counterpart CH_3CCH in TMC-1 is $(1.1–1.3) \times 10^{14}$ cm^{-2} (Gratier et al. 2016; Cabezas et al. 2021). Therefore, in this study we confirm that the propargyl radical is thermalized to the gas kinetic temperature of TMC-1 and revise the abundance ratio CH_2CCH/CH_3CCH to nearly one.

There are other rotational transitions of CH_2CCH that lie in the frequency range covered by our Yebes 40 m and IRAM 30 m data. The two other transitions of ortho CH_2CCH that fall in the λ 3 mm band, the $4_{0,4}$–$3_{0,3}$ at 74.9 GHz and the $6_{0,6}$–$5_{0,5}$ at 112.3 GHz, are predicted to be as intense as the $5_{0,5}$–$4_{0,4}$. However, our data at these frequencies are not as sensitive as at 93.6 GHz, and thus the strongest hyperfine components of each transition are only marginally detected. System temperatures at 74.9 GHz and 112.3 GHz are higher than at 93.6 GHz, making the $5_{0,5}$–$4_{0,4}$ transition the most favorable for detection. There are also several lines of para CH_2CCH accessible. Two of them, the $2_{1,2}$–$1_{1,1}$ at 37.2 GHz and the $2_{1,1}$–$1_{1,0}$ at 37.8 GHz, lie in the Q band and are covered by our Yebes 40 m line survey, while two other transitions, the $5_{1,5}$–$4_{1,4}$ at 92.8 GHz and the $5_{1,4}$–$4_{1,3}$ at 94.4 GHz, lie in the λ 3 mm band and are covered by our IRAM 30 m telescope data. These lines are predicted to be less intense than those of ortho CH_2CCH and, thus, are more difficult to detect. In our data only the strongest hyperfine components of the $5_{1,5}$–$4_{1,4}$ and $5_{1,4}$–$4_{1,3}$ transitions are visible, and only barely. The S/N is, however, low, and we have thus not attempted to fit them.

4. Conclusions

We detected the $5_{0,5}$–$4_{0,4}$ transition of ortho CH_2CCH in TMC-1 using the IRAM 30 m telescope. The measured frequencies for ten hyperfine components of this transition are 0.2 MHz higher than the frequency predictions available in the CDMS catalog, a difference that is significant for radio-astronomical purposes. We carried out a new spectroscopic analysis of the rotational spectrum of CH_2CCH in order to provide accurate frequencies at millimeter wavelengths. The intensity of the $5_{0,5}$–$4_{0,4}$ transition, lying at 93.6 GHz, is ∼5 times higher in TMC-1 than the $2_{0,2}$–$1_{0,1}$ previously observed by Agúndez et al. (2021a) using the Yebes 40 m telescope. We conclude that a search for CH_2CCH in other cold interstellar sources should be carried out in the λ 3 mm band (rather than at λ 8 mm), where the telescope time investment is estimated to be about seven times cheaper. The rotational temperature of CH_2CCH in TMC-1 is constrained to 9.9 ± 1.5 K (i.e., equal to the gas kinetic temperature), and the derived value of the column density is $(1.0 \pm 0.2) \times 10^{14}$ cm^{-2}, which makes CH_2CCH one of the most abundant hydrocarbon radicals in TMC-1.

Acknowledgements. We acknowledge funding support from Spanish Ministerio de Ciencia e Innovación through grants PID2019-106110GB-I00, PID2019-107115GB-C21, and PID2019-106235GB-I00 and from the European Research Council (ERC Grant 610256: NANOCOSMOS). M.A. also acknowledges funding support from the Ramón y Cajal programme of Spanish Ministerio de Ciencia e Innovación (grant RyC-2014-16277). We thank the referee for a careful reading of the manuscript and for useful comments.

References

Agúndez, M., Cabezas, C., Tercero, B., et al. 2021a, A&A, 647, L10
Agúndez, M., Marcelino, N., Tercero, B., et al. 2021b, A&A, 649, L4
Botschwina, P., Oswald, R., Flügge, J., & Horn, M. 1995, Z. Phys. Chem., 188, 29
Burkhardt, A. M., Lee, K. L. K., Changala, P. B., et al. 2021, ApJ, 913, L18
Cabezas, C., Endo, Y., Roueff, E., et al. 2021, A&A, 646, L1

Cernicharo, J. 1985, IRAM Internal Report 52
Cernicharo, J., Marcelino, N., Roueff, E., et al. 2012, ApJ, 759, L43
Cernicharo, J., Marcelino, N., Agúndez, M., et al. 2020, A&A, 642, L8
Cernicharo, J., Agúndez, M., Cabezas, C., et al. 2021a, A&A, 647, L2
Cernicharo, J., Cabezas, C., Agúndez, M., et al. 2021b, A&A, 647, L3
Cernicharo, J., Agúndez, M., Cabezas, C., et al. 2021c, A&A, 649, L15
Cernicharo, J., Agúndez, M., Kaiser, R. I., et al. 2021d, A&A, 652, L9
Cernicharo, J., Agúndez, M., Kaiser, R. I., et al. 2021e, A&A, 655, L1
Cordiner, M. A., Buckle, J. V., Wirström, E. S., et al. 2013, ApJ, 770, 48
Fehér, O., Tóth, L. V., Ward-Thompson, D., et al. 2016, A&A, 590, A75
Fossé, D., Cernicharo, J., Gerin, M., & Cox, P. 2001, ApJ, 552, 168
Gratier, P., Majumdar, L., Ohishi, M., et al. 2016, ApJS, 225, 25
Küpper, J., Merritt, J. M., & Miller, R. E. 2002, J. Chem. Phys., 117, 647
Marcelino, N., Cernicharo, J., Agúndez, M., et al. 2007, ApJ, 665, L127
McGuire, B. A., Burkhardt, A. M., Kalenskii, S., et al. 2018, Science, 359, 202
McGuire, B. A., Burkhardt, A. M., Loomis, R. A., et al. 2020, ApJ, 900, L10
McGuire, B. A., Loomis, R. A., Burkhardt, A. M., et al., 2021, Science, 371, 1265
Miller, J. A., & Klippenstein, S. J. 2001, J. Phys. Chem. A, 105, 7254
Müller, H. S. P., Schlöder, F., Stutzki, J., & Winnewisser, G. 2005, J. Mol. Struct., 742, 215
Pickett, H. M. 1991, J. Mol. Spectr., 148, 371
Pardo, J. R., Cernicharo, J., & Serabyn, E. 2001, IEEE Trans. Antennas Propag., 49, 1683
Pratap, P., Dickens, J. E., Snell, R. L., et al. 1997, ApJ, 486, 862
Tanaka, K., Sumiyoshi, Y., Ohshima, Y., et al. 1997, J. Chem. Phys., 107, 2728
Tercero, F., López-Pérez, J. A., Gallego, et al. 2021, A&A, 645, A37
Zhao, L., Lu, W., Ahmed, M., et al. 2021, Sci. Adv., 7, eabf0360